Metasurface Color Filters Using Aluminum and Lithium Niobate Configurations

Yu-Sheng Lin[*], Jie Dai, Zhuoyu Zeng and Bo-Ru Yang[*]

Abstract

Two designs of metasurface color filters (MCFs) using aluminum and lithium niobate (LN) configurations are proposed and numerically studied. They are denoted as tunable aluminum metasurface (TAM) and tunable LN metasurface (TLNM), respectively. The configurations of MCFs are composed of suspended metasurfaces above aluminum mirror layers to form a Fabry-Perot (F-P) resonator. The resonances of TAM and TLNM are red-shifted with tuning ranges of 100 nm and 111 nm, respectively, by changing the gap between the bottom mirror layer and top metasurface. Furthermore, the proposed devices exhibit perfect absorption with ultra-narrow bandwidth spanning the whole visible spectral range by composing the corresponding geometrical parameters. To increase the flexibility and applicability of proposed devices, TAM exhibits high sensitivity of 481.5 nm/RIU and TLNM exhibits high figure-of-merit (FOM) of 97.5 when the devices are exposed in surrounding environment with different refraction indexes. The adoption of LN-based metasurface can enhance FWHM and FOM values as 10-fold and 7-fold compared to those of Al-based metasurface, which greatly improves the optical performance and exhibits great potential in sensing applications. These proposed designs provide an effective approach for tunable high-efficiency color filters and sensors by using LN-based metamaterial.

Keywords: Metasurface, Tunable color filter, Lithium niobite

Introduction

Recently, the research progresses of metamaterials have advanced toward the realization of tunable metasurfaces that enables real-time control over their geometrical and optical properties, thus creating exceptional opportunities in the field of actively tunable metamaterials. They have been reported to span the visible [1–6], infrared (IR) [7–12], and terahertz (THz) [12–21] spectral ranges. As the unique optical properties in metasurfaces rely on the interaction between incident light and the nanostructure, desirable properties can be achieved by properly tailoring the shape, size, and composition of structure. Metasurfaces have enabled manipulation of near-field entities thereby allowing reconfiguration of intriguing features like magnetic response [1, 22], near-perfect absorption [14, 15, 23], transparency [17, 19], phase engineering [18, 20, 21, 24], MIR

sensing and thermal imaging [10], resonance modulation [9] for many types of filters [1–5], and sensors [6–8, 12–14] applications.

To date, there are many active tuning mechanisms reported to improve the flexibility of metasurface. Most of designs are in the IR [10–12, 25–27] and THz [28–31] spectral ranges. Although there have been various reported approaches for actively tunable metasurfaces in the visible spectral range, such as mechanical stretching [32], electrostatic force [33], Mie resonance [34], liquid crystal [35], phase change material [36–38], and electro-optic material [39, 40] However, the number of studies on actively tunable metasurfaces in the visible spectral range is limited. Among the tuning mechanisms of electro-optical methods, graphene-based tunable metasurface recently draws a massive attention to researchers [41–43]. Besides, lithium niobate (LN) is one of the most important materials, which is regarded as the "silicon of photonics." The approaches of metasurface on LN have drawn great attentions due to its wide transparency

* Correspondence: linyoush@mail.sysu.edu.cn; yangboru@mail.sysu.edu.cn
State Key Laboratory of Optoelectronic Materials and Technologies, School of Electronics and Information Technology, Sun Yat-Sen University, Guangzhou 510275, China

window, large second-order electro-optic coefficient up to 30 pm/V, and great compatibility with integrated photonics circuits [44]. Owing to its large second-order nonlinear susceptibility, the refraction index of LN can be tuned linearly by applying an electric field on it [44]. The incorporation of LN into the design of metasurface opens up the possibilities for ultrasensitive color filters with electro-optical active tunability. The above-mentioned active tuning methods are highly dependent on the nonlinear properties of natural material. They often lack desirable characteristics, such as large tuning range and uniform performance across the tuning range or requiring high drive voltage which severely limits their applications. Among these methods, actively tunable metamaterials using micro-electro-mechanical systems (MEMS) technology are widely studied due to the geometric characteristics of the metamaterial can be directly modified [26, 29]. MEMS-based tunable metamaterials often utilize a Fabry-Perot (F-P) cavity and then change the gap between two structural layers to tune the resonance [37, 45]. These structures can produce narrow absorption or transmission bandwidth with a large tuning range which makes it desirable for next generation applications.

In this study, two designs of metasurface color filters (MCFs) are presented. They are tunable Al-based metasurface (TAM) and tunable LN-based metasurface (TLNM) by using Lumerical Solution's finite difference time domain (FDTD)-based simulations to investigate their optical characteristics in the visible spectral range. The propagation direction of incident light is set to be perpendicular to the x–y plane in the numerical simulations. The polarization angle of incident light is set as 0 and it means the electric vector oscillates along the x-axis direction as TM polarization. Periodic boundary conditions are also adopted in the x and y directions, and perfectly matched layer (PML) boundary conditions are assumed in both z directions. The reflection intensity is calculated by a monitor set above the device. The proposed devices exhibit active tunabilities and large tuning ranges. TAM and TLNM exhibit near-perfect ultra-narrowband absorptions spanning the whole visible spectral range. For the environmental sensing application, TAM exhibits high sensitivity while TLNM exhibits high FOM. These designs can be potentially used in high-resolution display, refraction index sensor and adaptive device in the visible spectral range.

Designs and Methods

Figure 1a shows the schematic drawings of proposed TAM and TLNM. They are composed of suspended rectangular Al and elliptical LN metasurfaces on Si substrate coated with an Al mirror layer atop. The gap between the bottom Al mirror layer and the top metasurface can be tuned by using MEMS technology to form a F-P cavity between these two layers. The corresponding geometrical dimensions are the length of the rectangular hole in Al metasurface and two axes of the elliptical hole in LN metasurface along x-direction (D_x) and y-direction (D_y), the periods along x-direction (P_x) and y-direction (P_y), the thickness of metasurface (t), and the gap between the metasurface and the bottom
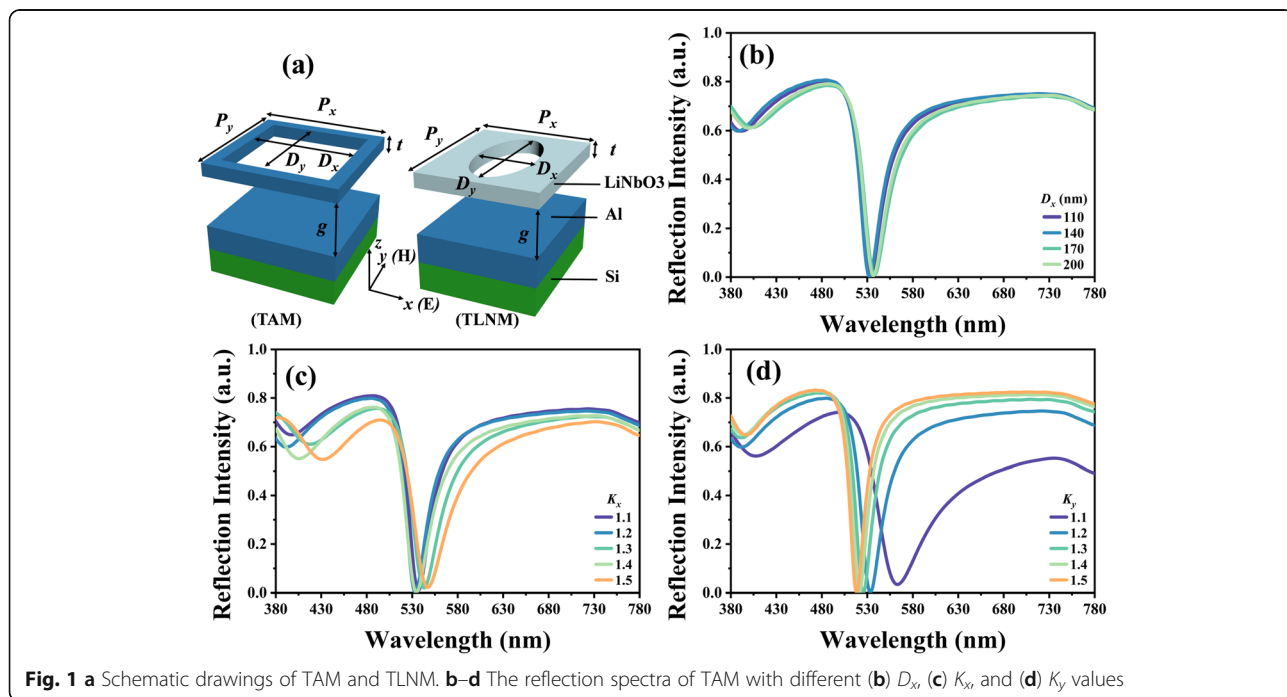

Fig. 1 **a** Schematic drawings of TAM and TLNM. **b**–**d** The reflection spectra of TAM with different (**b**) D_x, (**c**) K_x, and (**d**) K_y values

mirror layer (g). Here, we define the ratios of periods and the lengths of the rectangular Al metasurface and elliptical LN metasurface along x-direction and y-direction as $K_x = P_x/D_x$ and $K_y = P_y / D_y$, respectively, to figure out the effective electromagnetic responses in the whole visible spectral range.

Figure 1b–d shows the reflection spectra of TAM by changing D_x, K_x, and K_y values, respectively. In Fig. 1b, the parameters are kept as constant as $D_y = 200$ nm, $g = 450$ nm, and $K_x = K_y = 1.2$. The near-perfect absorption spectra are maintained by changing D_x values from 110 nm to 200 nm. The resonance is at the wavelength of 535 nm. Figure 1c shows the reflection spectra of TAM with different K_x values. Other parameters are kept as constant as $D_x = D_y = 200$ nm, $g = 450$ nm and $K_y = 1.2$. The resonances are almost kept as constant in the wavelength range of 530 nm to 540 nm. Figure 1d shows the reflection spectra of TAM with different K_y values. The other parameters are kept as constant as $D_x = D_y = 200$ nm, $g = 450$ nm and $K_x = 1.2$. By changing K_y values from 1.1 to 1.5, the resonances are blue-shifted with a varying wavelength range of less than 60 nm. These results indicate that the impacts of D_x, K_x, and K_y values on the resonant wavelength of TAM are quite minor, which means that the proposed TAM possesses a high tolerance of manufacturing deviation for the variations of D_x, K_x, and K_y values. In the following discussions, K_x and K_y are kept as constant as 1.2 and D_x is set to be equal to D_y to investigate the active tunability of the proposed TAM and TLNM devices.

Results and Discussions

To increase the flexibility and applicability of proposed device, the metasurface is designed to be suspended so as to leave a gap between itself and the bottom mirror layer to form a F-P resonator and as a result of which, the incident light will be trapped in this gap and then absorbed by the device. Regarding to the D_y and g values are the main factors contributing to the shift of resonant wavelength, near-perfect absorption of TAM can be

tuned in the whole visible spectral range by pairing D_y and g values as shown in Fig. 2a. Four pairs of D_y and g values are chosen to investigate the tunability of TAM. They are $(D_y, g) = (160$ nm, 355 nm$)$, $(200$ nm, 450 nm$)$, $(240$ nm, 540 nm$)$, $(280$ nm, 645 nm$)$, respectively. By composing of D_y and g values, the perfect absorption can be realized at different wavelengths of 433.9 nm, 533.5 nm, 629.8 nm, and 740.9 nm. The inserted color images of Fig. 2a are the corresponding visible colors of reflection spectra to human eyes calculated by using CIE RGB matching functions to imitate the real colors on device surfaces. The relationship of resonances and D_y values is summarized and plotted in Fig. 2b. The resonances are red-shifted linearly spanning the whole visible spectral range by increasing D_y values from 150 nm to 290 nm. The corresponding correction coefficient is 0.99401. It shows a great tunability for the proposed TAM device. The resonant frequency of a F-P resonator can be determined by [46]

$$v_q = \frac{qc}{2g} \tag{1}$$

where q is mode index, g is the length of F-P cavity, and $c = c_0 /n$, where c_0 is the speed of light in vacuum and n is refraction index of the medium. This indicates that resonant frequency can be tuned by moving the suspended metasurface vertically in this proposed design, i.e., changing the g value.

Figure 3 shows the reflection spectra of TAM with different g values under the conditions of $D_y = 200$ nm (Fig. 3a) and $D_y = 250$ nm (Fig. 3b), respectively. In Fig. 3a, the resonances are red-shifted from the wavelength of 490 nm to 590 nm by changing g values from 410 nm to 510 nm. The tuning range is 100 nm. The narrowest full width at half maximum (FWHM) of resonance is 29.9 nm for $g = 470$ nm. In Fig. 3b, the resonances are red-shifted from the wavelength of 580 nm to 691 nm by changing g values from 490 nm to 610 nm. The tuning
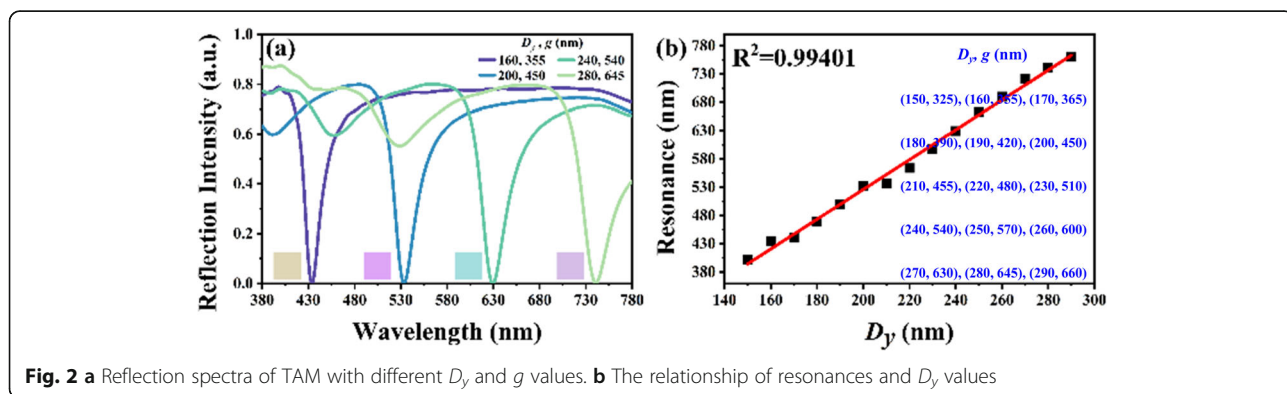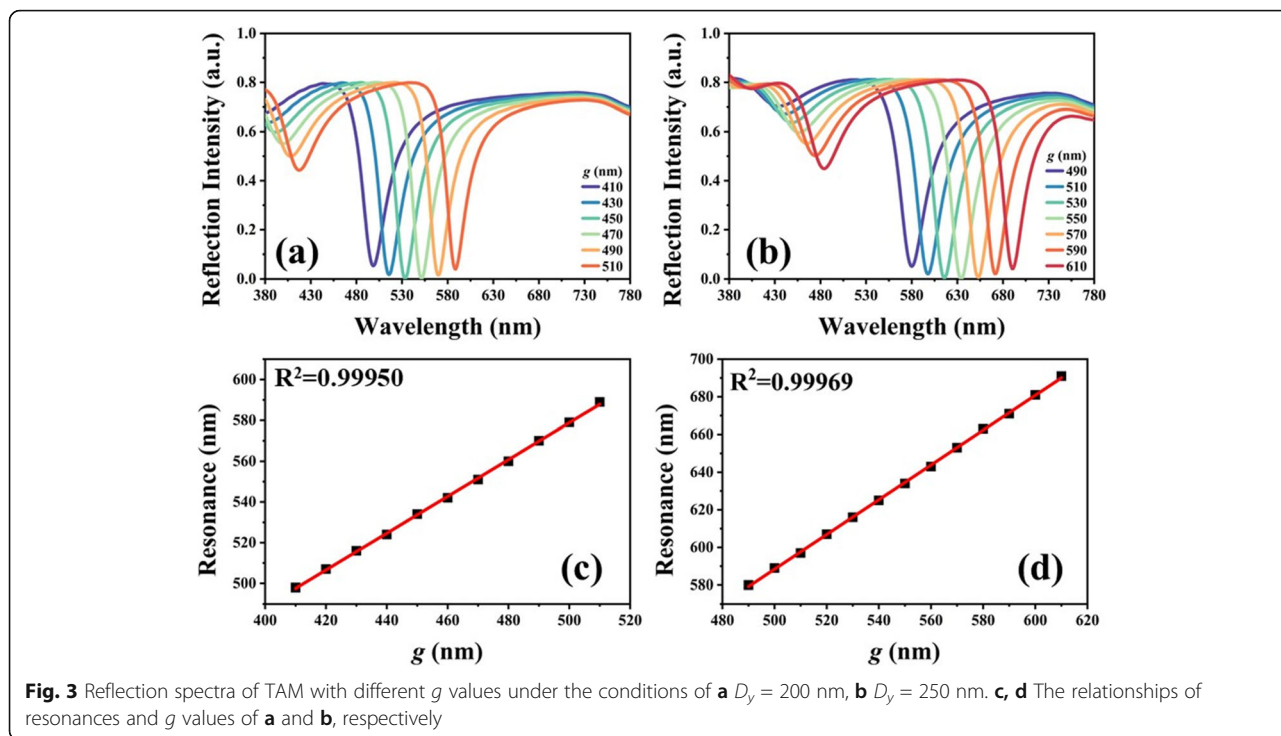

Fig. 2 a Reflection spectra of TAM with different D_y and g values. **b** The relationship of resonances and D_y values

Fig. 3 Reflection spectra of TAM with different g values under the conditions of **a** D_y = 200 nm, **b** D_y = 250 nm. **c, d** The relationships of resonances and g values of **a** and **b**, respectively

range is 111 nm. The narrowest FWHM of resonance is 31.8 nm for g = 530 nm. The tuning range is 2-fold compared to that reported in the reference [39] and better than those reported in the references previously [37, 38, 40]. Figure 3c, d shows the corresponding relationships of resonances and g values of Fig. 3a, b, respectively. The resonances are red-shifted linearly by 9.2 nm per 10 nm increment of g value as shown in Fig. 3c, and by 9.0 nm per 10 nm increment of g value as shown in Fig. 3d. The tuning ranges are 90.5 nm and 110.7 nm, respectively. All reflection spectra are near-perfect absorptions. The corresponding correction coefficients are 0.99950 and 0.99969, respectively. Such designs of proposed TAM may serve as an ultrasensitive color filter or be used in various sensing applications.

To improve the performance of TAM in terms of FWHM and the tuning wavelength range while keeping the near-perfect absorption, TLNM is proposed and presented as shown in Fig. 1a. It is because the patterning of nanostructures always suffers the corner effect and fabrication deviation that the geometrical pattern is designed as elliptical hole. The parameters of D_x and D_y represent the lengths of macro-axis and minor-axis along x- and y-directions, respectively, while K_x and K_y parameters are kept as constant as 1.2 and D_x value is 110 nm. Figure 4a shows the reflection spectra of TLNM with four combinations of D_y and g values. t value is kept as constant as 200 nm. TLNM exhibits the characteristic of perfect absorption with an ultra-narrow bandwidth spanning the whole visible spectral range. The FWHM values of reflection spectra are 3 nm. Such

Fig. 4 a Reflection spectra of TLNM with different D_y and g values. **b** The relationship of resonances and D_y values
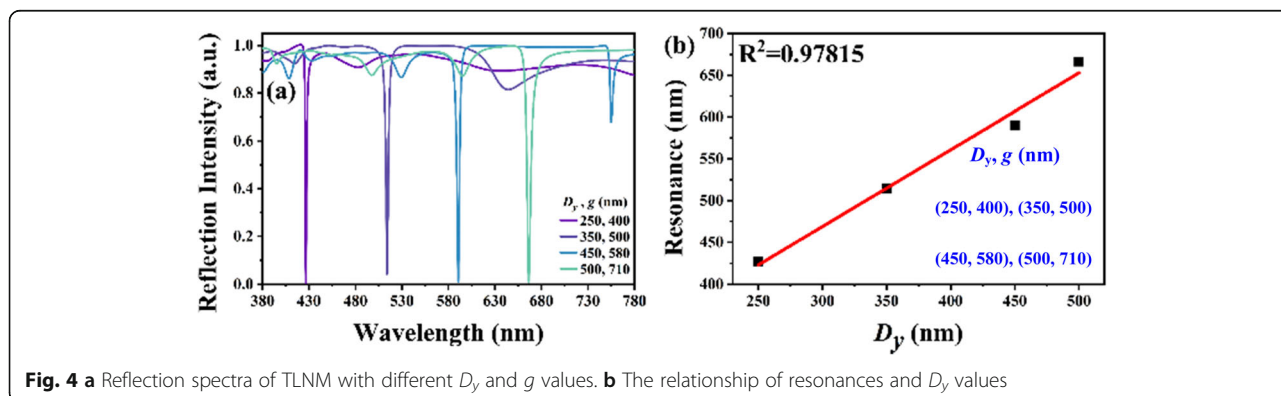
ultra-narrow FWHM is contributed by the F-P resonance, which can be determined by

$$\text{FWHM} = \frac{\lambda_q^2}{2\pi g}\frac{1-R}{\sqrt{R}} \qquad (2)$$

where λ_q is resonant wavelength, the subscript q is the mode index, g is the length of F-P cavity, and R is the reflectance of F-P resonator surfaces between bottom Al metasurface and Al/LN metasurface atop. FWHM value could be reduced as a result of higher reflection intensity of TLNM, which means the optical performance can be greatly improved by using LN material. The relationship of resonances and D_y values in Fig. 4a are summarized as shown in Fig. 4b. The resonances are red-shifted linearly spanning from 427 nm to 673 nm by increasing D_y values from 250 nm to 500 nm, and the corresponding correction coefficient is 0.97815. Hence, it demonstrates a linear tunability of the proposed device.

The suspended elliptical LN metasurface is moveable, which can be directly modified to achieve optical tunability by using MEMS technology. Figure 5a, b shows the reflection spectra of TLNM with different g values under two conditions of D_y = 350 nm, t = 210 nm, and D_y = 450 nm, t = 280 nm, respectively. In Fig. 5a, by increasing g values from 390 nm to 570 nm, the resonances are red-shifted from 465.9 nm to 553.5 nm. In Fig. 5b, by increasing g values from 540 nm to 780 nm, the resonances are red-shifted from 613.6 nm to 731.2

nm. Figure 5c, d shows the corresponding relationships of resonances, g values, and the corresponding FWHM values of Fig. 5a, b, respectively. The resonances are red-shifted quite linearly. The corresponding correction coefficients are 0.99864 and 0.99950 for two cases, respectively. For the case of D_y = 350 nm, t = 210 nm, the tuning range is 87.6 nm and the average FWHM value is 3 nm as shown in Fig. 5c. While for the case of D_y = 450 nm, t = 280 nm, the tuning range is 117.6 nm and the average FWHM value is 4 nm as shown in Fig. 5d. It can be seen the narrowest FWHM value is 1.5 nm at the wavelength of 466 nm as shown in Fig. 5a and that is 3.2 nm at the wavelength of 615 nm as shown in Fig. 5b. They are compared with the results of proposed TAM designs, the FWHM values of TLNM are improved 10-fold at least keeping the perfect absorption. It is a great improvement of optical performance by using LN metasurface. These results indicate that TLNM can be potentially used in many applications such as ultrasensitive color filters, absorbers, detectors, and sensors according to these extraordinary characteristics of ultra-narrowband, perfect absorption, and large tuning range.

To further investigate whether TAM and TLNM devices can be implanted into practical applications, e.g., environment sensors, they are exposed in the surrounding environment with different ambient refraction indexes (n). Figure 6 shows the reflection spectra of TAM exposed in surrounding environment with different refraction indexes from 1.0 to 1.3. The geometrical dimensions of TAM are kept as constant as D_x = 110 nm, D_y = 200 nm, and g = 450 nm.
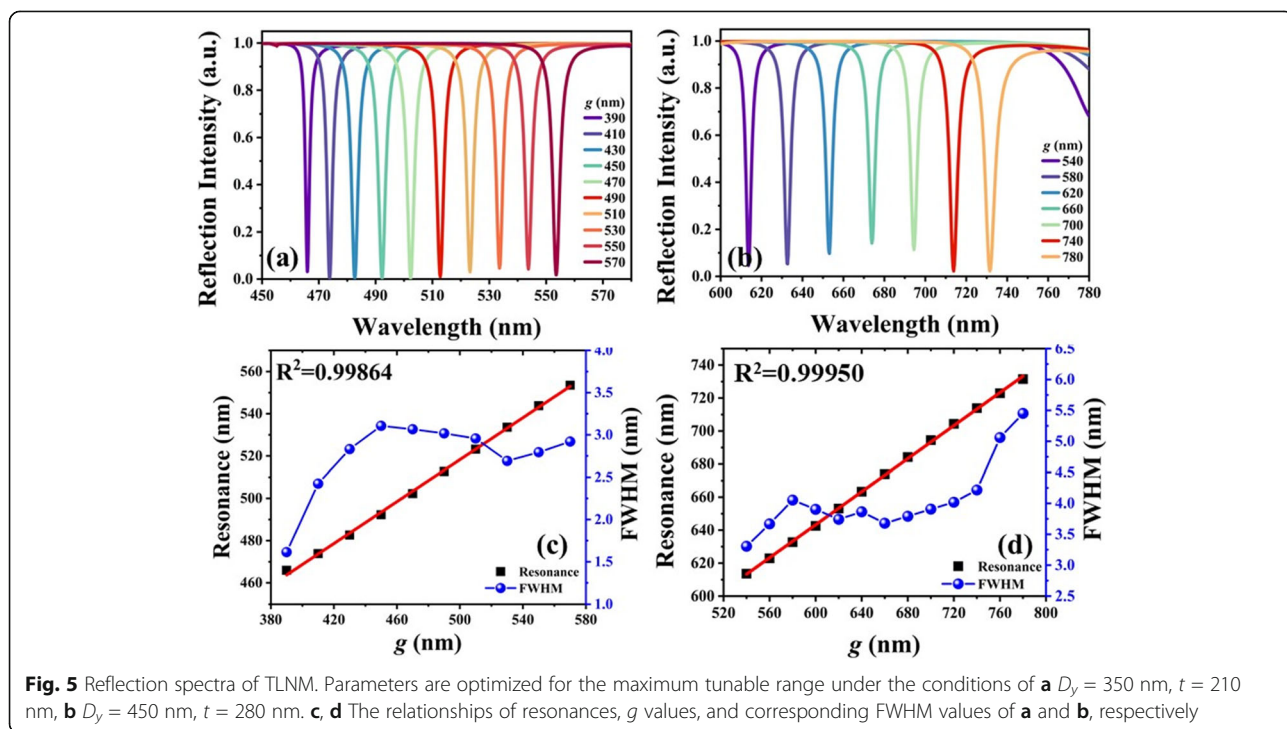

Fig. 5 Reflection spectra of TLNM. Parameters are optimized for the maximum tunable range under the conditions of **a** D_y = 350 nm, t = 210 nm, **b** D_y = 450 nm, t = 280 nm. **c**, **d** The relationships of resonances, g values, and corresponding FWHM values of **a** and **b**, respectively

Fig. 6 a Reflection spectra of TAM exposed in surrounding environment with different refraction indexes (*n*). **b** The relationship of resonances and *n* values
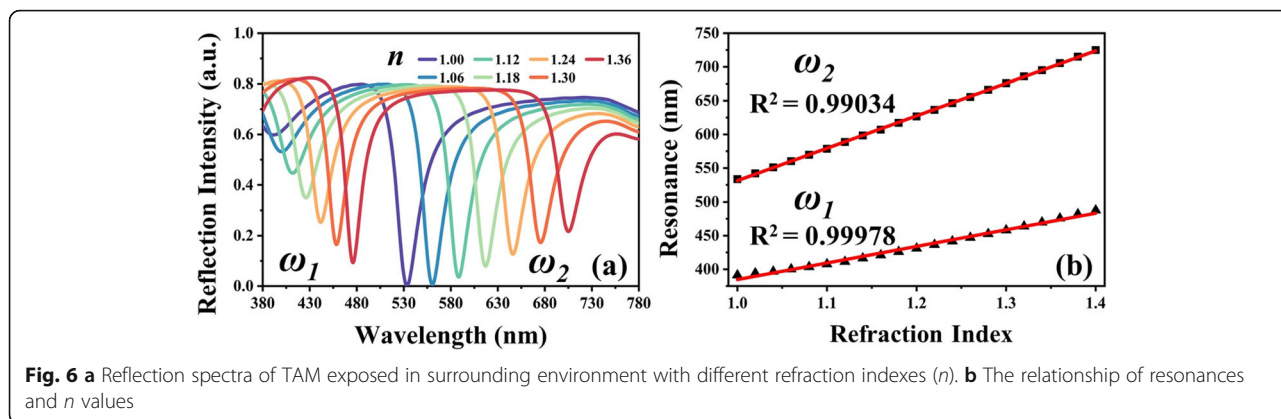
There are two resonances red-shifted with tuning ranges of 84.6 nm (ω_1) and 172.1 nm (ω_2). The relationships of resonances and *n* values are summarized in Fig. 6b. The sensitivities are calculated as 246.7 nm/RIU and 481.5 nm/RIU, and the corresponding figure-of-merits (FOMs) are 11 and 14 for the first resonance (ω_1) and second resonance (ω_2), respectively. These higher sensitivities are caused from the narrow FWHM of resonances, which are 21.6 nm (ω_1) and 34 nm (ω_2). These characteristics are quite suitable for pragmatic sensing applications.

However, the drawback is that the reflection intensity of ω_1 is relatively high and that of ω_2 increases to greater than 20% as *n* increases to 1.3. To overcome this limitation, TLNM is designed to possess the stable optical properties owing to the characterizations of LN metasurface. Figure 7

shows the reflection spectra of TLNM exposed in surrounding environment with different *n* values under the conditions of D_y = 350 nm, *t* = 210 nm, *g* = 490 nm, and D_y = 450 nm, *t* = 280 nm, *g* = 580 nm as shown in Fig. 7a, b, respectively. In Fig. 7a, the resonances of TLNM with D_y = 350 nm, *t* = 210 nm, *g* = 490 nm are red-shifted with a tuning range of 58.4 nm by increasing *n* values from 1.0 to 1.2. While the resonances of TLNM under the conditions of D_y = 450 nm, *t* = 280 nm, *g* = 580 nm are red-shifted with a tuning range of 78.2 nm by increasing *n* values from 1.0 to 1.2. Within these two cases, TLNM exhibits near-perfect absorption, where the fluctuation of reflection intensity is less 5%. The reflection spectra are more stable than those of TAM. The relationships of resonances and *n* values are plotted in Fig. 7c, d for the two cases,
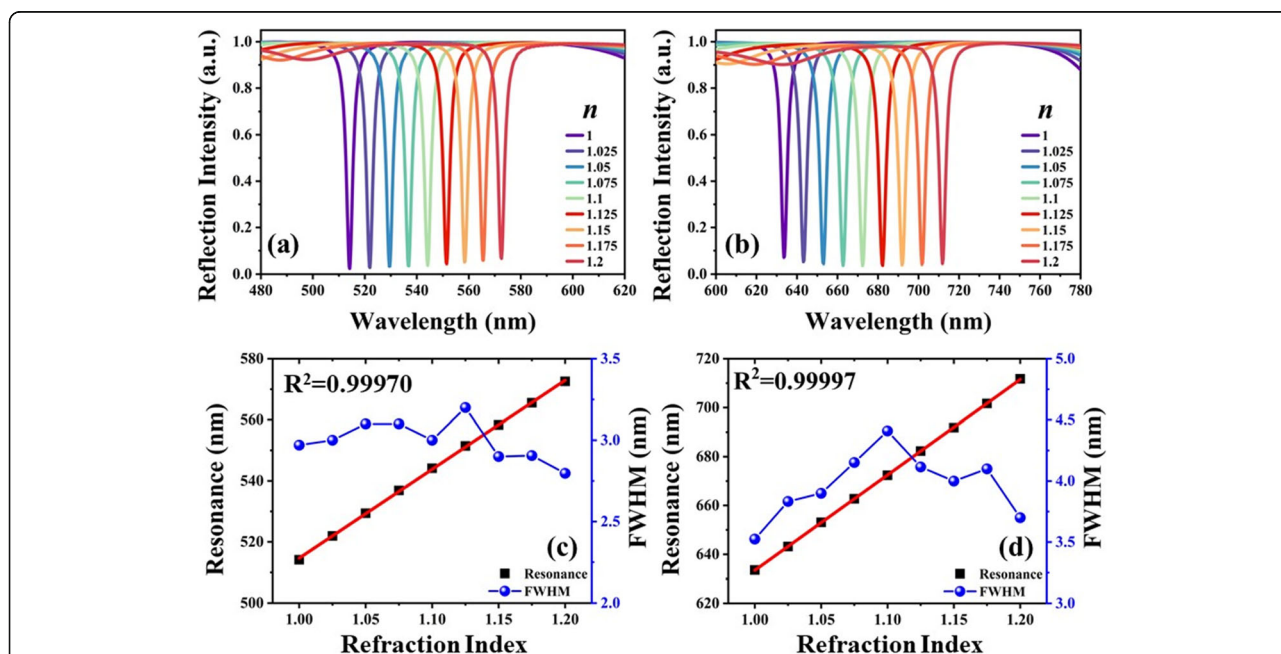

Fig. 7 Reflection spectra of TLNM exposed in surrounding environment with different refraction indexes (*n*) under the conditions of **a** D_y = 350 nm, *t* = 210 nm, *g* = 490 nm, **b** D_y = 450 nm, *t* = 280 nm, *g* = 580 nm. **c, d** The relationships of resonances, *n* values and corresponding FWHM values, respectively

Lin *et al. Nanoscale Research Letters* (2020) 15:77

Page 7 of 8

respectively. For the condition of TLNM with D_y = 350 nm, t = 210 nm, g = 490 nm, the sensitivity and the average FWHM value are 291.4 nm/RIU and 3 nm, respectively. The corresponding FOM is calculated as 97 as shown in Fig. 7c. For the condition of TLNM with D_y = 450 nm, t = 280 nm, g = 580 nm, the sensitivity and the average FWHM value are 390.3 nm/RIU and 4 nm, respectively. The corresponding FOM is calculated as 97.5 as shown in Fig. 7d, which is enhanced 7-fold compared to that of TAM shown in Fig. 6. It means that TLNM shows better sensing performance to be used in the environmental sensor applications.

Conclusion

In conclusion, we present two designs of tunable high-efficiency color filter based on suspended rectangular Al and elliptical LN metasurfaces on Si substrate coated with an Al mirror layer atop. By altering different compositions of D_x, g, and t values of TAM and TLNM, the electromagnetic responses can perform perfect absorption with ultra-high efficiency spanning the whole visible spectral range. By increasing g values, the resonances of TAM and TLNM can be tuned 110.7 nm and 117.6 nm, respectively. For the environmental sensing application, TAM exhibits ultra-high sensitivity of 481.5 nm/RIU and TLNM exhibits ultra-high FOM value of 97.5. The FWHM of TLNM is enhanced 10-fold at maximum and FOM can be improved by 7-fold compared those of TAM. According to the above-mentioned characteristics of ultra-narrowband, especially FWHM of 3 nm for TLNM, perfect absorption and a large tuning range which are rarely reported in the visible spectrum simultaneously by implanting Al or LN metasurface, it indicates that proposed devices can be potentially used in many applications such as ultrasensitive color filters with high color purity, high resolution for display and imaging techniques, high-efficiency tunable absorbers desirable in integrated optics, refraction index sensors, etc. Among these applications, TLNM exhibits a performance with higher FOM and narrower FWHM while TAM possesses a higher sensitivity for refraction index sensors.

Abbreviations
MCFs: Metasurface color filters; LN: Lithium niobate; TAM: Tunable aluminum metasurface; TLNM: Tunable LN metasurface; F-P: Fabry-Perot; FOM: Figure-of-merit; IR: Infrared; THz: Terahertz; FDTD: Finite difference time domain; PML: Perfectly matched layer

Authors' Contributions
JD and ZZ carried out the related experiments and data analysis. ZZ and YSL drafted the manuscript. YSL supervised the experiments and the revising of the manuscript. JD and YSL also provided suggestions and guidance for the experiments and data analysis. All authors read and approved the final manuscript.

Availability of Data and Materials
All data generated or analyzed during this study are included in this published article.

Competing Interests
The authors declare that they have no competing interests.

References
1. Pinton N, Grant J, Collins S, Cumming DRS (2018) Exploitation of magnetic dipole resonances in metal-insulator-metal plasmonic nanostructures to selectively filter visible light. ACS Photonics 5(4):1250–1261
2. Li Z, Clark AW, Cooper JM (2016) Dual color plasmonic pixels create a polarization controlled nano color palette. ACS Nano 10(1):492–498
3. Sun S, Zhou Z, Zhang C, Gao Y, Duan Z, Xiao S, Song Q (2017) All-dielectric full-color printing with TiO2 metasurfaces. ACS Nano 11(5):4445–4452
4. Huang Y, Zhu J, Fan J, Chen Z, Chen X, Jin S, Wu W (2019) Plasmonic color generation and refractive index sensing with three-dimensional air-gap nanocavities. Opt Express 27(5):6283–6299
5. Lee SU, Ju BK (2017) Wide-gamut plasmonic color filters using a complementary design method. Sci. Rep. 7:40649
6. Zhou W, Li K, Song C, Hao P, Chi M, Yu M, Wu Y (2015) Polarization-independent and omnidirectional nearly perfect absorber with ultra-thin 2D subwavelength metal grating in the visible region. Opt Express 23(11): A413–A418
7. Hwang I, Yu J, Lee J, Choi JH, Choi DG, Jeon S, Lee J, Jung JY (2018) Plasmon-enhanced infrared spectroscopy based on metamaterial absorbers with dielectric nanopedestals. ACS Photonics 5(9):3492–3498
8. Chong X, Zhang Y, Li E, Kim KJ, Ohodnicki PR, Chang CH, Wang AX (2018) Surface-enhanced infrared absorption: pushing the frontier for on-chip gas sensing. ACS Sens. 3(1):230–238
9. Petronijevic E, Leahu G, Di Meo V, Crescitelli A, Dardano P, Coppola G, Esposito E, Rendina I, Miritello M, Grimaldi MG, Torrisi V, Compagnini G, Sibilia C (2019) Near-infrared modulation by means of GeTe/SOI-based metamaterial. Opt Lett 44(6):1508–1511
10. Dong B, Luo X, Zhu S, Hu T, Li M, Hasan D, Zhang L, Chua SJ, Wei J, Chang Y, Ma Y, Vachon P, Lo GQ, Ang KW, Kwong DL, Lee C (2019) Thermal annealing study of the mid-infrared aluminum nitride on insulator (AlNOI) photonics platform. Opt Express 27:19815–19826
11. Dong B, Luo X, Zhu S, Li M, Hasan D, Zhang L, Chua SJ, Wei J, Chang Y, Lo GQ, Ang KW, Kwong DL, Lee C (2019) Aluminum nitride on insulator (AlNOI) platform for mid-infrared photonics. Opt Lett 44:73–76
12. Ren Z, Chang Y, Ma Y, Shih K, Dong B, Lee C (2019) Leveraging of MEMS Technologies for Optical Metamaterials Applications. Adv Optical Mater: 1900653
13. Shih K, Pitchappa P, Jin L, Chen C-H, Singh R, Lee C (2018) Nanofluidic terahertz metasensor for sensing in aqueous environment. Appl Phys Lett 113(7):071105
14. Wang W, Yan F, Tan S, Zhou H, Hou Y (2017) Ultrasensitive terahertz metamaterial sensor based on vertical split ring resonators. Photonics Res 5(6):571–577
15. Zhao X, Wang Y, Schalch J, Duan G, Cremin K, Zhang J, Chen C, Averitt RD, Zhang X (2019) Optically Modulated Ultra-Broadband All-Silicon Metamaterial Terahertz Absorbers. ACS Photonics 6(4):830–837
16. Zhou Z, Zhou T, Zhang S, Shi Z, Chen Y, Wan W, Li X, Chen X, Gilbert Corder SN, Fu Z, Chen L, Mao Y, Cao J, Omenetto FG, Liu M, Li H, Tao TH (2018) Multicolor T-Ray Imaging Using Multispectral Metamaterials. Adv Sci 5(7):1700982
17. Liu C, Li H, Xu H, Zhao M, Xiong C, Zhang B, Wu K (2019) Slow light effect based on tunable plasmon-induced transparency of monolayer black phosphorus. J Phys D 52(40):405203

Lin *et al. Nanoscale Research Letters*   (2020) 15:77

Page 8 of 8

18. Yangjian Z, Chuhuan F, Qi L, Xin S, Hongbin Y (2019) Dynamic Reflection Phase Modulation in Terahertz Metamaterial. IEEE Photon J 11(4):4601212
19. Yahiaoui R, Manjappa M, Srivastava YK, Singh R (2017) Active control and switching of broadband electromagnetically induced transparency in symmetric metadevices. Appl Phys Lett 111(2):021101
20. Cong L, Pitchappa P, Wu Y, Ke L, Lee C, Singh N, Yang H, Singh R (2017) Active multifunctional microelectromechanical system metadevices: applications in polarization control, Wavefront Deflection, and Holograms. Adv Optical Mater 5(2):1600716
21. Ma F, Qian Y, Lin YS, Liu H, Zhang X, Liu Z, Tsai JML, Lee C (2013) Polarization-sensitive microelectromechanical systems based tunable terahertz metamaterials using three dimensional electric split-ring resonator arrays. Appl Phys Lett 102:161912
22. Hu X, Wei X (2017) Metallic metasurface for high efficiency optical phase control in transmission mode. Opt Express 25(13):15208–15215
23. Liu X, Jia X, Fischer M, Huang Z, Smith DR (2018) Enhanced two-photon photochromism in metasurface perfect absorbers. Nano Lett 18(10):6181–6187
24. Zhao XG, Zhang JD, Fan KB, Duan GW, Schalch J, Keiser GR, Averitt RD, Zhang X (2019) Real-time tunable phase response and group delay in broadside coupled split-ring resonators. Phys Rev B 99(24):245111
25. Yi Z, Lin H, Niu G, Chen XF, Zhou ZG, Ye X, Duan T, Yi Y, Tang YJ, Yi YG (2019) Graphene-based tunable triple-band plasmonic perfect metamaterial absorber with good angle-polarization-tolerance. Results Phys. 13:102149
26. Reeves JB, Jayne RK, Stark TJ, Barrett LK, White AE, Bishop DJ (2018) Tunable infrared metasurface on a soft polymer scaffold. Nano Lett. 18(5):2802–2806
27. Pitchappa P, Manjappa M, Krishnamoorthy HNS, Chang Y, Lee C, Singh R (2017) Bidirectional reconfiguration and thermal tuning of microcantilever metamaterial device operating from 77 K to 400 K. Appl Phys Lett 111(26):261101
28. Manjappa M, Pitchappa P, Wang N, Lee C, Singh R (2018) Active Control of Resonant Cloaking in a Terahertz MEMS Metamaterial. Adv Opt Mater 6(16):1800141
29. Manjappa M, Pitchappa P, Singh N, Wang N, Zheludev NI, Lee C, Singh R (2018) Reconfigurable MEMS Fano metasurfaces with multiple-input-output states for logic operations at terahertz frequencies. Nat Commun 9(1):4056
30. Shih KL, Pitchappa P, Manjappa M, Ho CP, Singh R, Yang B, Singh N, Lee C (2017) Active MEMS metamaterials for THz bandwidth control. Appl Phys Lett 110(16):161108
31. Huang X, Yang F, Gao B, Yang Q, Wu J, He W (2019) Metamaterial absorber with independently tunable amplitude and frequency in the terahertz regime. Opt Express 27(18):25902–25911
32. Tseng ML, Yang J, Semmlinger M, Zhang C, Nordlander P, Halas NJ (2017) Two-dimensional active tuning of an aluminum plasmonic array for full-spectrum response. Nano Lett. 17(10):6034–6039
33. Honma H, Mitsudome M, Ishida M, Sawada K, Takahashi K (2017) Nano-optomechanical characterization of surface-plasmon-based tunable filter integrated with comb-drive actuator. J Micromech Microeng 27(3):034001
34. van de Groep J, Brongersma ML (2018) Metasurface mirrors for external control of mie resonances. Nano Lett. 18(6):3857–3864
35. Olson J, Manjavacas A, Basu T, Huang D, Schlather AE, Zheng B, Halas NJ, Nordlander P, Link S (2016) High chromaticity aluminum plasmonic pixels for active liquid crystal displays. ACS Nano 10(1):1108–1117
36. Gholipour B, Piccinotti D, Karvounis A, MacDonald KF, Zheludev NI (2019) Reconfigurable ultraviolet and high-energy visible dielectric metamaterials. Nano Lett. 19(3):1643–1648
37. Song SC, Ma XL, Pu MB, Li X, Guo YH, Gao P, Luo XG (2018) Tailoring active color rendering and multiband photodetection in a vanadium-dioxide-based metamaterial absorber. Photonics Res. 6(6):492–497
38. Bakan G, Ayas S, Saidzoda T, Celebi K, Dana A (2016) Ultrathin phase-change coatings on metals for electrothermally tunable colors. Appl Phys Lett 109(7):071109
39. Bibbò L, Khan K, Liu Q, Lin M, Wang Q, Ouyang Z (2017) Tunable narrowband antireflection optical filter with a metasurface. Photonics Res. 5(5):500–506
40. Mirshafieyan SS, Gregory DA (2018) Electrically tunable perfect light absorbers as color filters and modulators. Sci Rep 8(1):2635
41. Rodrigo D, Limaj O, Janner D, Etezadi D, de Abajo FJG, Pruneri V, Altug H (2015) Mid-infrared plasmonic biosensing with graphene. Science 349(6244):165–168
42. Zhu H, Chen S, Wen J, Wang J, Chen L (2019) Graphene-based metasurfaces for switching polarization states of anomalous reflection and focusing. Opt Lett. 44(23):5764–5767
43. Zhu H, Deng M, Chen S, Chen L (2019) Graphene-based meta-coupler for direction-controllable emission of surface plasmons. Opt Lett 44(13):3382–3385
44. Wang C, Zhang M, Stern B, Lipson M, Loncar M (2018) Nanophotonic lithium niobate electro-optic modulators. Opt Express 26(2):1547–1555
45. Lo CY, Huttunen OH, Hiitola-Keinanen J, Petaja J, Fujita H, Toshiyoshi H (2010) MEMS-controlled paper-like transmissive flexible display. J Microelectromech Syst. 19(2):410–418
46. Ismail N, Kores CC, Geskus D, Pollnau M (2016) Fabry-Pérot resonator: spectral line shapes, generic and related airy distributions, linewidths, finesses, and performance at low or frequency-dependent reflectivity. Opt Express 24(15):16366–16389

Publisher's Note

Springer Nature remains neutral with regard to jurisdictional claims in published maps and institutional affiliations.